Cancer Management and Research

Dovepress

open access to scientific and medical research

Open Access Full Text Article

ORIGINAL RESEARCH

RETRACTED ARTICLE: Long Non-Coding RNA ZNF667-AS1 Knockdown Curbs Liver Metastasis in Acute Myeloid Leukemia by Regulating the microRNA-206/AKAP13 Axis

This article was published in the following Dove Press journal:
Cancer Management and Research

Nan Wang*
Yanping Feng*
Jinye Xie
Hui Han
Qian Dong
Weijia Wang

Laboratory Diagnosis Center, Zhongshan People's Hospital, Zhongshan, 528403 Guangdong, People's Republic of China

*These authors contributed equally to this work

Background: Zinc finger protein 667-antisense RNA 1 (*ZNF667-AS1*), a long non-coding RNA (lncRNA), plays important part in tumorigenesis and development of esophageal squamous cell carcinoma, but its function in acute myeloid leukemia (AML) is unknown. Our goal here was to probe the functional mechanism of *ZNF667-AS1* in AML by mediating microRNA-206 (*miR-206*)/A-kinase anchoring protein 13 (*AKAP13*) axis.

Materials and Methods: The bone marrow samples from AML patients and controls were selected for microarray analysis to select significantly upregulated lncRNAs. Next, effects of *ZNF667-AS1* on cell aggressiveness of AML were assessed after delivery of cells with siRNA against *ZNF667-AS1*. Subcellular fractionation location assay and FISH experiments were used to determine *ZNF667-AS1* localization in cells. Dual-luciferase experiments detect the targeting relationships among *ZNF667-AS1*, *miR-206* and *AKAP13*. Finally, tumor growth and metastasis were evaluated in vivo to determine the relevance of *ZNF667-AS1*/*miR-206*/*AKAP13* axis.

Results: The expression of *ZNF667-AS1* was upregulated in AML patients, which predicted poor prognosis. Downregulation of *ZNF667-AS1* reduced cell proliferation, invasion, tumorigenesis and metastasis. *miR-206* inhibitor reversed the repressive role of *ZNF667-AS1* knockdown in cell proliferation, invasion and tumorigenesis, while *AKAP13* silencing flattened the stimulative role of *miR-206* inhibitor in AML malignant aggressiveness. Mechanistically, we demonstrated that *ZNF667-AS1* functioned as a molecular sponge for *miR-206*. In addition, we observed that Wnt/β-catenin pathway was suppressed by *ZNF667-AS1* knockdown.

Conclusion: *ZNF667-AS1* potentiated AML progression by targeting the *miR-206*/*AKAP13* axis. This indicates *ZNF667-AS1* inhibition may act as a prospective therapeutic option for the treatment of AML.

Keywords: long non-coding RNA *ZNF667-AS1*, *microRNA-206*, *AKAP13*, acute myeloid leukemia

Introduction

Acute myeloid leukemia (AML) has the characteristics of clonal expansion of undifferentiated myeloid precursors, contributing to disrupted hematopoiesis and bone marrow failure.[1] AML diagnosed in older adults (age ≥ 60 years) often have dismal prognoses, with long-term overall survival rates of only 5–16%.[2] Treatments for AML include at least one course of intensive chemotherapy, followed by another course of

Correspondence: Weijia Wang
Email jiaweiw3311@163.com

intensive consolidation therapy as well as maintenance therapy.[3] However, AML is still lethal in about half of younger patients and in approximately 80% of elderly patients due to primary refractoriness, relapse, or treatment-associated mortality.[4] Moreover, approximately only one third of patients over the age of 60 are eligible for intensive chemotherapy.[5] Because of the limitations of current therapies, effective and individualized treatments are urgently needed for patients with AML.

Long non-coding RNAs (LncRNAs) differentiate themselves from short non-coding RNA by longer lengths, varying from 200 to 100,000 nucleotides, which could communicate with other RNA transcripts using a language composed of microRNA (miRNA) response elements.[6] For instance, SOCS2-AS promoted AML cell proliferation by regulating STAT5 through miR-221.[7] Another lncRNA, zinc finger protein 667-antisense RNA 1 (*ZNF667-AS1*) has been reported to act as a tumor suppressor by regulating ANK2/JAK2 expression or targeting miR-93-3p/PEG3 axis in colorectal cancer and cervical cancer, which were both solid tumors.[8,9] More relevantly, higher gene expression of *ZNF667-AS1* exceeding the cutoff value has been found to be associated with unsatisfactory overall survival for patients suffered from B-chronic lymphocyt leukemia.[10] Nevertheless, little information is available on the roles of *ZNF667-AS1* in AML. Interestingly, *miR-206* expression in bone marrow and serum of pediatric AML sufferers were remarkably decreased than their counterparts, and poor *miR-206* expression in the serum was tightly linked to unfavorable clinicopathologic characteristics and prognosis of pediatric AML patients.[11] Hence, we postulated that *ZNF667-AS1* might participate in the progression of AML by interacting with *miR-206*. The integrated online prediction and dual-luciferase experiments revealed that A-kinase anchor proteins 13 (*AKAP13*) is a direct and putative target of *miR-206*. *AKAP13*, also known as lymphoid blast crisis oncogene (LBC), breast cancer nuclear receptor binding auxiliary protein gene (BRX), and catalytic GDP-GTP exchange factor (GEF), has been validated as a tumor-supporting gene in colorectal cancer.[12] *AKAP13* increased the resistance of AML patients to tipifarnib by about 5 to 7 folds.[13] Given the aforementioned evidence, we conjectured that the poor survival of AML patients may be associated with *ZNF667-AS1* upregulation and the underlying molecular mechanisms in relation to *miR-206*-mediated *AKAP13* expression.

Materials and Methods

Patients and Clinical Samples

From September 2014 to September 2016, 86 AML patients in Zhongshan People's Hospital were enrolled, including 38 males and 48 females. Bone marrow samples used for diagnoses were collected for experiments. Patients were diagnosed with AML on the basis of French American British (FAB) and World Health Organization criteria and were classified into M1-M6 subtypes according to blood and bone marrow patterns. The clinicopathological features are listed in Table 1. A total of 25 bone marrow samples from non-AML patients receiving bone marrow examination and bone marrow donation was recruited as controls. AML patients had an average age of 51 and the control (CON) group 45. The protocols of the current study were permitted by the Ethics Committee of Zhongshan People's Hospital following the Declaration of Helsinki. All participants signed written informed consent forms before enrollment.

Microarray-based Gene Analysis

The bone marrow samples from six AML patients by stratified random sampling (one for each stage in M1-M6) were subjected to lncRNA analysis. Bone marrow samples from six age- and sex-matched subjects were set as the control group. GeneChip human Gene 2.0 ST Arrays (Affymetrix, Thermo Fisher Scientific Inc., Waltham, MA, USA) were used for lncRNA microarray analysis.

Table 1 Clinical Characteristics Between AML Patients and Controls

Groups	Control (n = 25)	AML (n = 86)
Sex (male/female)	14/9	38/48
Age (Year)	43.58 ± 7.64	51.26 ± 9.18
WBC ($\times 10^9$/L)	5.21 ± 1.18	80.91 ± 69.28
HGB (g%)	16.22 ± 4.25	7.15 ± 2.46
PLT ($\times 10^9$/L)	250.5 ± 23.58	60.21 ± 13.72
LDH (U/L)	211.86 ± 23.55	407 ± 34.79
Present FAB subtype		
M1	NA	11
M2	NA	24
M3	NA	13
M4	NA	19
M5	NA	14
M6	NA	5

Abbreviations: AML, acute myeloid leukemia; WBC, white blood count; HGB, hemoglobin; PLT, platelets; LDH, lactate dehydrogenase; FAB, French American British; NA, not applicable.

Affymetrix GeneChip Scanner 3000 7G was used to analyze significant changes of gene expression profiles under 570 nm wavelength excitation, and Partek Genomic Suite 6.6 software was utilized for statistical screening (Partek Incorporated, St. Louis, MI, USA). Robust multiple-array average (RMA) algorithm was used to normalize the gene array files on the core meta-sample set. The gene expression was analyzed by fold discovery rate, and the heatmap was plotted to screen upregulated lncRNAs with Foldchange value greater than 2 and $p < 0.01$. The detailed data are provided in Supplementary Material.

RT-qPCR

Total RNA was isolated from tissues and cells using Trizol reagents (Invitrogen Inc., Carlsbad, CA, USA). Complementary DNA (cDNA) was synthesized using PrimeScript Real-time Reagent kits with gDNA Eraser (TaKaRa, Shiga, Japan). Then, SYBR premix (Takara) was applied to detect *ZNF667-AS1* expression and the mRNA expression of *AKAP13* using glyceraldehyde-3-phosphate dehydrogenase (GAPDH) as an internal reference. The expression of miR-206 was detected using miRNA RT-qPCR Detection kits (Genecopoeia, Rockville, MD, USA) with U6 as an internal ref[illegible] PCR reactions were performed on ABI 7500 Real[illegible]ime PCR System (Applied Biosystems, Inc., Foster City, [illegible] USA), and the gene expression was m[illegible]sured [illegible]sing t[illegible] $2^{-\Delta\Delta Ct}$ method. The primers used in [illegible]his stu[illegible] are pre[illegible]sented in Table 2.

Cell Culture and Tr[illegible]atment

Human AML cells U[illegible]7, THP-1, [illegible]60, NB4, normal bone marrow cells [illegible]S-5 and HEK2931 cells were purchased from BeNa[illegible]ulture [illegible]ollection (Beijing, China). No phenotypic v[illegible]iation a[illegible] mycopl[illegible]ma contamination were identified. U937 and T[illegible]R cells were cultivated in Roswe[illegible]Park M[illegible]orial Institute-1640 medium (Solarbio, Beijing, C[illegible]). HL60, NB4 and HS-5 cells were grown in Dulbecco's [illegible]dified Eagle's medium (DMEM, Gibco, Carlsbad, CA, USA) added with 10% fetal bovine serum (FBS, Hyclone, Marlborough, MA, USA) and 2 mM L-glutamine (Hyclone). Small interfering RNAs (siRNAs) targeting *ZNF667-AS1* (*ZNF667-AS1* si) and *AKAP13* (*AKAP13* si), *miR-206* inhibitor (*miR-206* inh), nonsense control sequence NC si (control for *ZNF667-AS1* si), NC (nonsense mRNA sequence for *miR-206* inh and *AKAP13* si) and packaging vector Helper vector-I were from GenePharma (Shanghai, China). Cells were transfected

Table 2 Sequences of RT-qPCR Primer

Targets	Sequences (5′-3′)
ZNF667-AS1	Forward: GGGAGTGTCCGCCATAAAGT
	Reverse: AGATCGTAGCAGGGTCCAGT
miR-206	Forward: AGATCGTAGCAGGGTCCAGT
	Reverse: CTGCAGGGTCCGAGGT
AKAP13	Forward: GAGAGTGTACCTCAAAACAAGGTGT
	Reverse: TTAAAATCTGGGAGAGAGACACATC
U6	Forward: GTCTCCT[illegible]TCAACAGCG
	Reverse: ACCA[illegible]CTGTTGCT[illegible]AGCCAA
GAPDH	Forward: [illegible]TTCG[illegible]AGCACA[illegible]TACTAAAAT
	Rev[illegible]e: CGCT[illegible]CACGA[illegible]GCGTGTCAT

Abbreviations: RT-[illegible]CR, [illegible]ers[illegible]transcriptio[illegible]quantitative polymerase chain reaction; ZNF667[illegible]1, zinc [illegible]er protei[illegible]67-antisense RNA 1; miR-206, microRNA-206[illegible]AP13, A-kina[illegible]ncho[illegible]g protein 13; GAPDH, glyceraldehyde-3-phos[illegible]te [illegible]drogenase.

[illegible]th these plasmids [illegible]or siRNA using Lipofectamine™ [illegible]000 transfe[illegible]ion reagent (Invitrogen). siRNAs and inhi[illegible]tor fragme[illegible]s used for transfection are shown in Table 3.

[illegible](4,5-Dimethylthiazal-2-Yl)-2,5-Diphenyl-Tetrazolium Bromide (MTT) Assay

Cells at logarithmic growth phase were seeded into 96-well plates at 1×10^4 cells/100 μL and cultured for 24, 48, 72 h, respectively, at 37°C. At indicated time points, 20 μL MTT solution (5 g/L, Sigma-Aldrich Chemical Company, St Louis, MO, USA) was added. After incubation for another 4 h, 150 μL dimethylsulfoxide was then

Table 3 Sequence for Cell Transfection

Targets	Sequence (5′–3′)
ZNF667-AS1 si-1	TGTGACAAGTTCTTCAGGCG
ZNF667-AS1 si-2	CTCTTTAACCAAACCCAACTA
*miR-206*inhibitor	CCACACACUUCCUUACAUUC
NC (for *ZNF667-AS1* si, *miR-206* inhibitor and AKAP si)	CAGUACUUUUGUGUAGUACA
AKAP si-1	GAGAAUGCAGAACGUUUPAA
AKAP si-2	GGAGAAGGAGAAAGATTCTTT

Abbreviations: ZNF667-AS1, zinc finger protein 667-antisense RNA 1; miR-206, microRNA-206; AKAP13, A-kinase anchoring protein 13; si, small interfering RNA.

supplemented to each well for a 15-min shaking in the dark. The optical density (OD) value of each well was read at 490 nm on a microplate reader (Multiskan MK3, Thermo).

5-Ethynyl-2′-Deoxyuridine (EdU) Staining

EdU assay kits (KeyGene, Rockville, MD, USA) were also adopted for cell proliferation assessment. Cells were seeded into 96-well plates at 5×10^3 cells/well, incubated with 10 μM EdU for 2 h, fixed with 4% formaldehyde for 20 min and cultured in 100 μL 0.5% TritonX-100 for 20 min. The cells were finally stained with Hoechst 33,342 (Beyotime, Shanghai, China) for 15 min and observed under a fluorescence microscopy (× 400, Olympus, Tokyo, Japan). The EdU activity of cells was assessed by counting EdU-positive cells.

Flow Cytometry

The cells in logarithmic growth phase were seeded in a 24-well plate (1×10^5 cells/well) for a 48-h culture. The cells were then suspended in 100 μL binding buffer from Annexin V-fluorescein isothiocyanate (FITC)/propidium iodide (PI) cell apoptosis kits (Sigma-Aldrich) and stained with 5 μL Annexin V-FITC and 5 μL PI for 10 min in darkness. The mixture was loaded onto a FACScan flow cytometer (BD Biosciences, San Jose, CA, USA).

Hoechst Staining

The transfected THP-1 and HL-60 cells were fixed with 4% paraformaldehyde for a period of 10 min and treated with 0.5 mL Hoechst 33,258 solution (Beyotime) for 10 min (both at room temperature). Following the addition of the anti-quencher, the cells were added dropwise onto the slides, and the apoptotic nuclei were observed using a fluorescence microscope (× 40, Olympus, Tokyo, Japan).

Transwell Invasion Assay

The inserts were coated using 50 μL Matrigel (Sigma-Aldrich). A total of 200 μL cell suspension was supplemented to apical chamber of the Transwell (8 μm pore diameter, Corning Glass Works, Corning, N.Y., USA), and 10% FBS-supplemented 300 μL DMEM to basolateral chamber for culturing in a 37°C incubator with 5% CO_2. After 48 h, the chambers were immersed in 4% paraformaldehyde for 30 min, 0.2% Triton X-100 (Sigma-Aldrich) for 15 min and 0.5% crystal violet for 5 min. Five randomly selected fields were observed with an inverted microscope (XDS-800D, Shanghai Caikon Optical Instrument, China) to assess cell invasion ability.

Xenograft Tumor in Nude Mice

Thirty-six 6-week-old female SD nude mice (weight 18 g ± 2 g) purchased from Shanghai SLAC Laboratory Animal (Shanghai, China) were allowed standard chow pellets and water ad libitum. A 12–12 h lights on-off cycle was maintained in a temperature-controlled room (22°C). Mice were randomly divided into 12 groups (n = 3 in each group) by weight after 1 week of acclimation through the injection of THP-1 or HL-60 cells transfected with siRNAs targeting *ZNF667-AS1* (*ZNF667-AS1* si) or negative control (NC-si), or cells co-transfected with *ZNF667-AS1* si + *miR-206* inhibitor (inh) or *miR-206* inh + siRNAs targeting *AKAP13* (*AKAP13* si) with *ZNF667-AS1* si + NC and *miR-206* inh + NC as controls. After 24 h post-infection, THP-1 and HL-60 cells were injected subcutaneously into the axilla of mice. The length and width of xenograft tumors were measured after one week of injection to calculate the tumor volume based on the formula: volume = $(a \times b^2)/2$, where "a" indicates length and "b" indicates width. After 4 weeks, mice were euthanized by an intraperitoneal injection of pentobarbital sodium at 150 mg/kg to dissect tumor tissues. All animal experiments were implemented with the approval of the Ethics Committee of Zhongshan People's Hospital. The report of animal experiments is in accordance with the ARRIVE guidelines.

In vivo Metastasis Experiments

Thirty-six 6-week-old female SD nude mice (weight 18 g ± 2 g) purchased from Shanghai SLAC Laboratory Animal were habituated to the housing conditions for one week. A total of 4×10^6 stably transfected AML cells were injected intravenously into the tail. After 45 d, mice were euthanized by intraperitoneal injection of sodium pentobarbital at 150 mg/kg. Liver tissues were removed and fixed in 4% paraformaldehyde, dehydrated with alcohol, embedded in paraffin and cut into 5-μm thick liver sections. After conventional dewaxing, the sections were treated with hematoxylin (Wuhan Boster Biological Technology, Wuhan, Hubei, China) for 3 min and stained with eosin for 3 min. Histopathological changes of liver tissues of mice were observed under microscope (XDS-800D, Shanghai Caikon Optical Instrument).

Immunohistochemistry

Mouse tumor tissues and liver nodules were routinely dewaxed after routinely embedding. The sections were allowed to stand with 3% H_2O_2 and with normal goat

serum blocking solution (for 15 min at room temperature). Sections were incubated with the primary antibody against CD45 (1:200, ab10558, Abcam, Cambridge, USA) overnight at 4°C, followed by incubation with the secondary antibody (1:2000, ab205718, Abcam) for 2 h at 37°C. Horseradish-labeled streptomyces ovalbumin working solution was added for 15-min color development at 37°C. The sections were then counterstained with hematoxylin for 30 s, dehydrated and sealed. The number of CD45-positive cells was observed under a microscope (XDS-800D, Shanghai Caikon Optical Instrument).

Subcellular Fractionation Location Assay

Cytoplasmic & Nuclear RNA Purification Kits (Norgen Biotek, Canada) were used to detect *ZNF667-AS1* localization in cells. The RNA of nucleus and cytoplasm was extracted, and cells were lysed using lysis buffer J and centrifuged. The precipitated pellets were added into adsorption columns. RNA was incubated at room temperature for 3 h with buffer and ethanol, and washed with hypotonic buffer to remove impurities. Then the RNA was isolated using Elution Buffer E by a 30-min incubation and centrifuged for 30 min at 15,000 ×g to separate nucleus and cytoplasm (both at 4°C). U6 was applied as a reference for nuclear RNA detection, and GAPDH was used as a reference for cytoplasmic RNA detection.

Fluorescence in situ Hybridization (FISH)

FISH was utilized to identify the subcellular localization of *ZNF667-AS1* in THP-1 and HL-60 cells. The cover slides were placed in 6-well culture plates, and THP-1 and HL-60 cells were seeded into plates according to Ribo™ lncRNA FISH probe Mix (Guangzhou RiboBio Co., Ltd., Guangzhou, Guangdong, China). After a 1-day culture, the cell confluence reached around 80%. The samples were then fixed at room temperature with 1 mL 4% paraformaldehyde and treated with protease K (2 μg/mL), glycine, and ethyl phthalide reagent. Afterwards, the cells were pre-hybridized with 250 μL pre-hybridization solution at 42°C for a period of 1 h and hybridized with 250 μL hybridization solution containing probe (300 ng/mL) at 42°C overnight. The nucleus was then stained with phosphate-buffered saline/Tween-diluted 4′,6-diamidino-2-phenylindole (1:800) for 5 min. Finally, cells were sealed with anti-fluorescent quencher. Focus was placed on five distinct areas, and the cells were counted under a fluorescence microscope (Olympus, Tokyo, Japan).

Luciferase Activity Detection

RNA22 (http://www.mybiosoftware.com/rna22-v2-microrna-target-detection.html) was used to predict the targeting miRNA of *ZNF667-AS1*. TargetScan (http://www.targetscan.org/vert_72/) was applied to predict the targeting mRNA of *miR-206*. Wild-type (WT) or mutated-type (MT) sequences of *ZNF667-AS1* or *AKAP13* containing predicted *miR-206* binding position were separately cloned into pMIRREPORT luciferase reporter vectors (Ambion, Austin, TX, USA). The transfection reagent lipofectamine™ 2000 was used to co-transfect those vectors with *miR-206* mimic or NC, respectively, into HEK-293T. Luciferase activity was detected using luciferase assay kits (Promega, Madison, WI, USA) and GloMax 20/20 machine (Promega) at 48 h post-transfection. Renilla luciferase activity was used for normalization.

Western Blot

Total proteins were extracted from tumor tissues and cells using radioimmunoprecipitation assay lysis buffer (Beyotime, Shanghai, China). Protein samples were subjected to 10% sodium dodecyl sulfate-polyacrylamide gel electrophoresis and transferred to polyvinylidene fluoride membranes (Millipore Corp, Billerica, MA, USA). After blocking nonspecific protein signaling using 5% skim milk, the membrane was incubated for 1 h under 4°C overnight with antibodies against β-catenin (ab16051, 1:500), cyclin D1 (ab16663,1:1000) and β-actin (ab8226,1:700) (all from Abcam, Cambridge, MA, USA) and with horseradish peroxidase-labeled secondary antibody (ab205719, 1:3000) at room temperature. Blots were detected using enhanced chemiluminescence detection kits (Pierce Biotechnology, Rockford, IL, USA). Data were analyzed using Image Quant LAS-4000 image acquisition system (FUJIFILM VisualSonics, Inc., Toronto, ON, Canada).

Statistical Analysis

Statistical analysis was conducted using GraphPad Prism 6.0 (GraphPad, San Diego, CA, USA) and SPSS 22.0 (IBM Corp, Armonk, NY, USA). Measurement data were displayed in the form of mean ± standard deviation (SD). Unpaired *t*-test was applied for analyses between two groups, and the comparison among multiple groups was analyzed by one-way or two-way analysis of variance (ANOVA), followed by Tukey's post hoc test. Survival curves were plotted using the Kaplan-Meier method and analyzed using the Log rank test. The effect of genes on the determination of AML progression in patients was determined by relative operating characteristic (ROC)

curves, and correlations between genes were performed by Person's test. Cox regression model univariate and multivariate analysis was used for survival evaluation. Differences were considered significant if the *p*-value was less than 0.05. The results shown were representative of at least three independent experiments.

Results

Upregulation of ZNF667-AS1 is Identified in AML Patients

Bone marrow from AML patients in Zhongshan People's Hospital and donated bone marrow from healthy controls (CON) were used for microarray analysis. The expression of *ZNF667-AS1* in bone marrow of AML patients increased significantly (Figure 1A), which was in consistence with results of RT-qPCR (Figure 1B). Since AML could be divided into M1-M6 subtypes according to the FAB classification, we tested the expression of *ZNF667-AS1* in the bone marrow of each subtype with the normal bone marrow as controls. RT-qPCR also validated that AML in each subtype was also increased relative to CON (Figure 1C). Through the survival analysis of the patients, the survival rate of patients with *ZNF667-AS1* high expression was observed to be lower (Figure 1D). ROC w used for the specificity of mRNAs in patients with AML t assess the efficiency of mRNA expression for the determination of AML. By ROC curve to detect the specificity of *ZNF667-AS1* in AML, we found that area under curve (AUC) was 0.75, indicating that *ZNF667-AS1* had good diagnostic efficiency for AML (Figure 1E). The expression of *ZNF667-AS1* in AML cell lines U937, THP-1, HL-60 and NB4 was detected with normal cells HS-5 as a control, and it was found that *ZNF667-AS1* was also significantly increased in AML cells (Figure 1F). Collectively, these results indicated that *ZNF667-AS1* may be a biomarker in AML.

Downregulation of ZNF667-AS1 Decreases AML Cell Activity

Since THP-1 and HL-60 cells show the relative high expression of *ZNF667-AS1*, we construct cells with *ZNF667-AS1* poor expression in THP-1 and HL-60 ce (Figure 2A). The proliferation ability of c was detected by MTT experiments, and the growth cur was p d with O values recorded on the 1st, 2nd and days, respe vel The OD values of AML cells after transfec n of *ZNF667-AS1* si plasmid were decrease suggesting duced proliferation (Figure 2B). Simi rly, we also assessed the DNA replication activity of cell by EdU stain g. The EdU-positive cells observed under a fluor scence mic scope were significantly reduced as well, indicative wered cell activity (Figure 2C). Meanwhile, ce re subjected to PI and Annexin V staining and then reened by flow cytometry. Late apoptotic cells were showed in the upper right quadrant, and cells were counted to assess

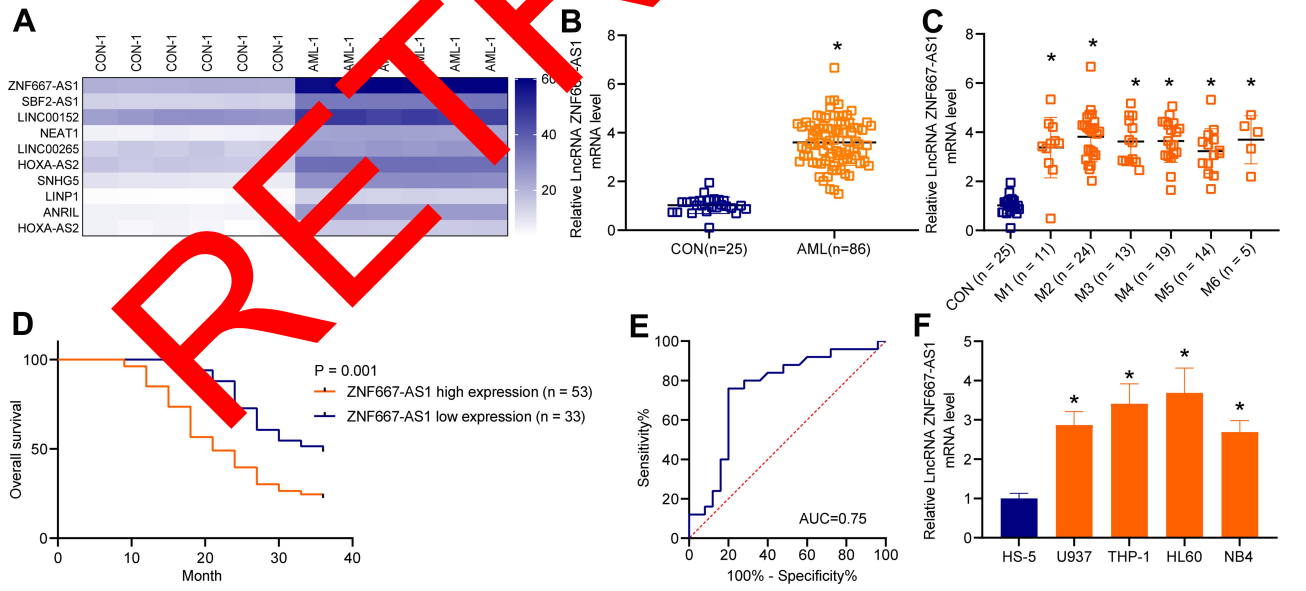

Figure 1 *ZNF667-AS1* is elevated in AML patients and cells. (**A**) Differentially expressed lncRNAs between CON and AML patients screened out by microarray analysis; (**B**) RT-qPCR detection of *ZNF667-AS1* expression in AML patients and CON (**p* < 0.05 according to the unpaired *t*-test); (**C**) RT-qPCR detection of *ZNF667-AS1* expression in AML patients of each subtype (**p* < 0.05 according to one-way ANOVA); (**D**) survival analysis of patients with high or low expression of *ZNF667-AS1* (cut-off value = 5.13); (**E**) ROC curve analysis for diagnostic efficiency of *ZNF667-AS1*; (**F**) RT-qPCR detection of *ZNF667-AS1* expression in AML cells and HS-5 cells (**p* < 0.05 according to one-way ANOVA). Values are shown as the means ± SD of three separate experiments.

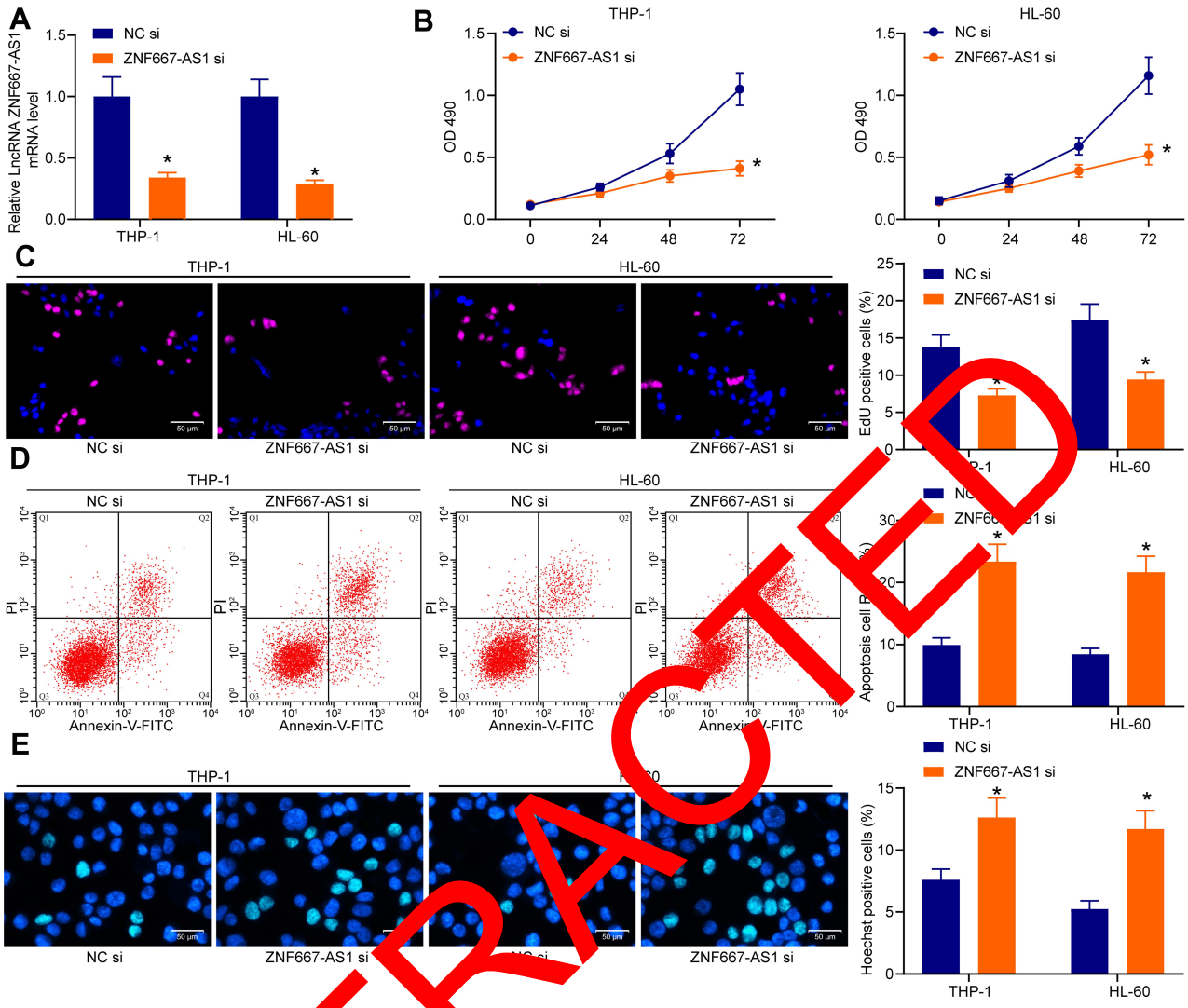

Figure 2 Downregulation of *ZNF667-AS1* reduces AML cell activity. NC si or *ZNF667-AS1* si was administrated into AML cells. (**A**) RT-qPCR detection of *ZNF667-AS1* expression in AML cells after transfection (*p < 0.05 according to two-way ANOVA); (**B**) MTT evaluation of cell OD value (*p < 0.05 according to one-way ANOVA); (**C**) EdU staining of cell proliferation (*p < 0.05 according to one-way ANOVA); (**D**) Flow cytometry of cell apoptosis ability (*p < 0.05 according to one-way ANOVA); (**E**) Hoechst staining for number of apoptotic cells (*p < 0.05 according to one-way ANOVA). Values are shown as the means ± SD of three separate experiments.

apoptotic activity. The poor expression of *ZNF667-AS1* contributed to a significant increment of double positive cells (Figure 2D). Consistent results were found by Hoechst staining as well (Figure 2E). In a word, these data suggested that *ZNF667-AS1* knockdown suppressed proliferation and increased apoptosis in AML.

Downregulation of ZNF667-AS1 Reduces Invasiveness of AML Cells

Transwell assays were employed to evaluate cell invasion ability in vitro. After 24 h of culture, the invasive cells were observed. Downregulation of *ZNF667-AS1* led to a decline in cell invasion number (Figure 3A). Cells transfected with plasmids containing *ZNF667-AS1* silencing fragment were injected into nude mice to observe tumor formation in vivo. The animal modeling was determined to be successful by detection of *ZNF667-AS1* expression. After confirming that the cell injection was effective (Figure 3B), tumor volume was assessed to evaluate the tumorigenic capacity of transfected cells. It was found that the tumor volume and weight of nude mice injected with cells transfected with *ZNF667-AS1* si plasmids were significantly smaller than that of the NC si group on the 28th days post-injection (Figure 3C). Immunohistochemical staining of a leukocyte marker CD45 in mouse tumor tissues revealed that the *ZNF667-AS1* reduced the CD45 expression and

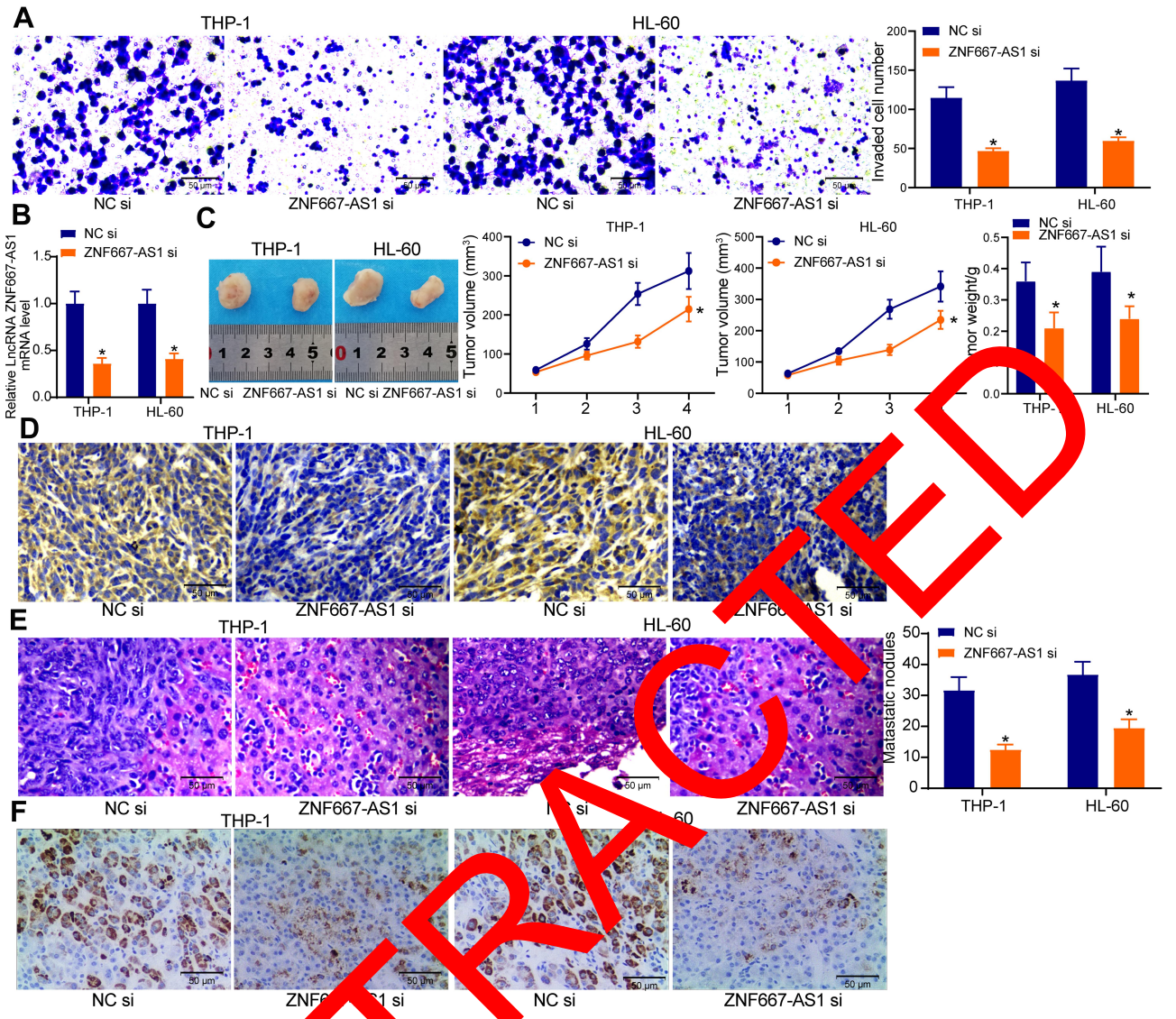

Figure 3 Downregulation of *ZNF667-AS1* reduces AML cell invasiveness in vitro and in vivo. NC si or *ZNF667-AS1* si was administrated into AML cells. (**A**) Transwell assay of cell invasion (*$p < 0.05$ according to one-way ANOVA); (**B**) RT-qPCR detection of *ZNF667-AS1* expression in mouse tumor tissues (*$p < 0.05$ according to one-way ANOVA); (**C**) Tumor volume and tumor weight in mice (*$p < 0.05$ according to one-way ANOVA); (**D**) Immunohistochemical staining of CD45 protein in mouse tumor tissues; (**E**) HE staining of liver metastatic nodules in mice (*$p < 0.05$ according to one-way ANOVA); (**F**) Immunohistochemical staining of CD45 protein in liver metastatic nodules. Values are shown as the means ± SD of three separate experiments (n = 3).

inhibited the expansion of AML cells (Figure 3D). HE staining was performed to observe the formation of liver metastatic nodules to assess the metastatic ability of mice, and the number of liver metastatic nodules was also significantly reduced (Figure 3E). The expression of the marker CD45 was also detected by immunohistochemistry in liver metastatic tissues, and *ZNF667-AS1* si was found to inhibit the formation of AML cells-derived liver metastatic nodules (Figure 3F). This series of results showed that *ZNF667-AS1* significantly reduced the invasive, tumorigenic and metastatic capacities of the AML cells.

miR-206 is Downregulated in AML Patients and Cells

The expression of *miR-206* was much lower in the bone marrow of AML patients than that in CON (Figure 4A). After typing the patients, the *miR-206* expression in all the patients were lower than that of the CON (Figure 4B). The correlation analysis of *miR-206* and *ZNF667-AS1* expression in patients showed that their expression in AML was negatively correlated (Figure 4C). Prognostic analysis of patients with different expression of *miR-206* revealed that the survival rate of patients with high expression of *miR-206* was higher, while that

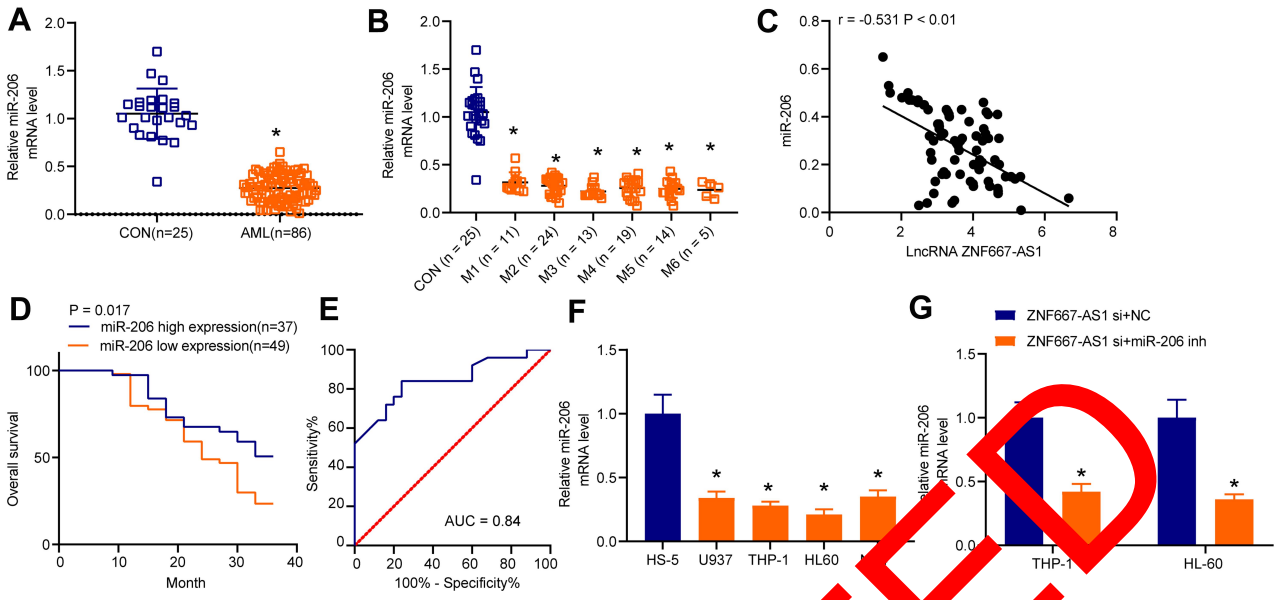

Figure 4 *miR-206* is reduced in AML patients and cell lines. (**A**) RT-qPCR detection of *miR-206* expressio[n] AML patients [a]nd CON[s] ($p < 0.05$ according to the unpaired *t*-test); (**B**) RT-qPCR detection of *miR-206* expression in AML patients of each subtype (*$p < 0.05$ accor[d]ing t[o] one-way ANOVA); (**C**) Correlation analysis of *ZNF667-AS1* and *miR-206* expression in AML patients; (**D**) Survival analysis of patients with high or low expression [o]f *miR-206* ([c]ut-off value = 0.91); (**E**) ROC curve analysis for diagnostic efficiency of *miR-206*; (**F**) RT-qPCR detection of *miR-206* expression in AML cells and HS-5 cells (*$p < 0.05$ accor[d]ing to one-way ANOVA); (**G**) RT-qPCR detection of *miR-206* expression in AML cells in the response to *ZNF667-AS1* si + *miR-206* inh (*$p < 0.05$ [a]ccording to two-way ANOVA). Values are shown as the means ± SD of three separate experiments.

of patients with poor expression of miR-206 was [l]ower (Figure 4D). The ROC curves involving *miR-206* expression found that *miR-206* also had good diagnostic efficiency in AML patients (Figure 4E). *miR-206* expression was then detected in AML and normal cells, which was found to be significantly reduced in AML cells (Figure 4F), suggesting that *miR-206* is also a candidate biomarker in AML. *miR-206* expression was also knocked-down in cells with *ZNF667-AS1* si. RT-qPCR assay manifested that the introduction of *miR-206* inhibitor led to a notable decline in *miR-206* expression in AML cells (Figure 4G). Therefore, *miR-206* was significantly downregulated in AML and may be a marker for AML.

miR-206 Inhibitor Reverses the Repressive Role of ZNF667-AS1 Inhibition in AML Cells

With simultaneous knockdown of *ZNF667-AS1* and *miR-206*, we detected cell proliferation by MTT, and found that OD values at 490 nm were increased (Figure 5A), suggesting a partial recovery of cell proliferation activity. We then used flow cytometry to detect the level of apoptosis, and observed that the number of apoptotic cells was decreased significantly after *ZNF667-AS1* si + *miR-206* inh treatment compared with *ZNF667-AS1* si alone (Figure 5B). *miR-206* inh also partially restored the invasive activity in the presence of *ZNF667-AS1* si (Figure 5C). To test the effect of *miR-206* on in vivo tumor growth and metastasis, we injected cells stably expressing *ZNF667-AS1* si + *miR-206* inh or *ZNF667-AS1* si + NC into nude mice. Poor expression of *miR-206* accelerated tumor growth (Figure 5D) and increased tumor weight (Figure 5E) in mice. Similarly, staining of CD45-positive cells revealed that leukocytes were significantly elevated after downregulation of *miR-206* (Figure 5F). HE staining of liver metastatic nodules showed that the metastatic nodule formation was significantly enhanced (Figure 5G). The levels of the leukocyte marker CD45 were also significantly enhanced in liver metastatic nodules (Figure 5H). Downregulation of *miR-206* inhibited the effects of *ZNF667-AS1* si, resulting in increased cell activity and enhanced tumorigenic capacity.

Upregulation of AKAP13 is Identified in AML Patients and Cells

*AKAP13*expression was upregulated in all AML patients (Figure 6A) and in each subtype of AML patients (Figure

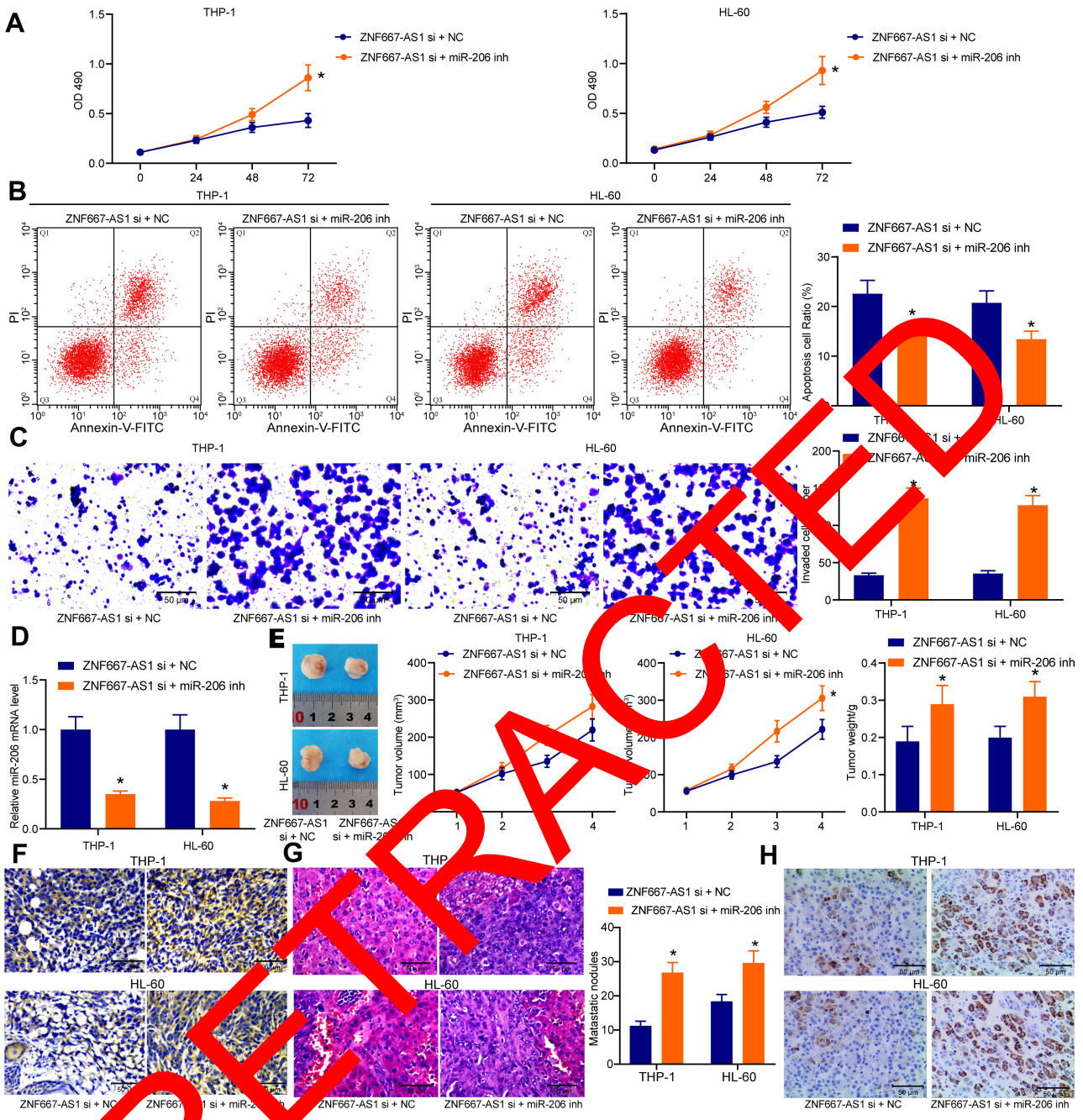

Figure 5 miR-20[illegible] inhibit[illegible] promote[illegible] AML cell aggressiveness in the presence of *ZNF667-AS1* silencing. (**A**) MTT evaluation of cell OD value (*$p < 0.05$ according to two-way ANOVA); (**B**) flow cytometry of cell apoptosis ability (*$p < 0.05$ according to two-way ANOVA); (**C**) Transwell assay of cell invasion (*$p < 0.05$ according to two-way ANOVA); (**D**) RT-qPCR detection of *miR-206* expression in mouse tumor tissues in the response to *ZNF667-AS1* si + *miR-206* inh (*$p < 0.05$ according to two-way ANOVA); (**E**) Tumor volume and tumor weight in mice (*$p < 0.05$ according to two-way ANOVA); (**F**) Immunohistochemical staining of CD45 protein in mouse tumor tissues; (**G**) HE staining of liver metastatic nodules in mice (*$p < 0.05$ according to two-way ANOVA); (**H**) Immunohistochemical staining of CD45 protein in liver metastatic nodules. Values are shown as the means ± SD of three separate experiments (n = 3).

6B). We observed a negative correlation between *AKAP13* and *miR-206* expression (Figure 6C) and a positive correlation between *ZNF667-AS1* and *AKAP13* expression (Figure 6D). The survival analysis of patients displayed that patients with high *AKAP13* expression had a poorer survival (Figure 6E), while the positive rate of *AKAP13* was higher and the diagnosis was better (Figure 6F). *AKAP13* expression was found to be significantly upregulated (Figure 6G) in AML cells, so we considered *AKAP13* to be an important biomarker in AML.

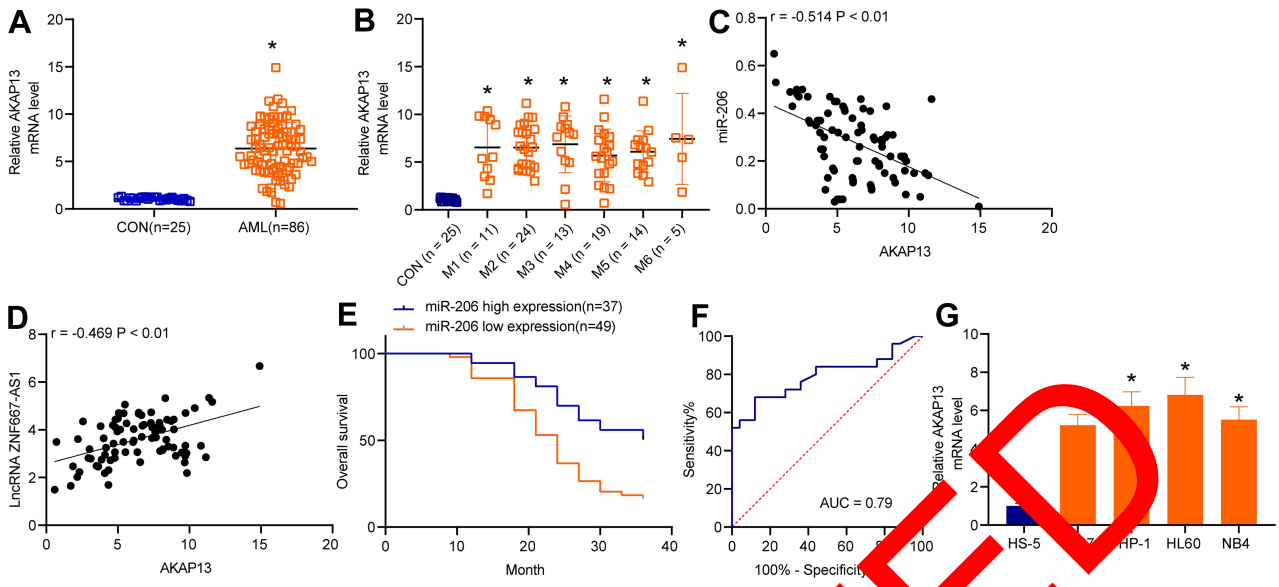

Figure 6 *AKAP13* is elevated in AML patients and cells. (**A**) RT-qPCR detection of *AKAP13* expression in AML patients and CON (*p < 0.05 according to the unpaired *t*-test); (**B**) RT-qPCR detection of *AKAP13* mRNA expression in AML patients of each subtype (*p < 0.05 according to one-way ANOVA); (**C**) correlation analysis of miR-206 and *AKAP13* expression in AML patients; (**D**) correlation analysis of *ZNF667-AS1* and *AKAP13* expression in AML patients; (**E**) survival analysis of patients with high or low expression of *AKAP13* (cut-off value = 5.84); (**F**) ROC curve analysis for diagnostic efficiency of *AKAP13*; (**G**) RT-qPCR detection of *AKAP13* mRNA expression in AML cells and HS-5 cells (*p < 0.05 according to one-way ANOVA). Values are shown as the means ± SD of three separate experiments.

Downregulation of AKAP13 Abrogates the Role of miR-206 Inhibitor in AML Cells

To detect the effect of *AKAP13* on the biological function of AML cells, we first constructed cells with poor expression of *miR-206*, and RT-qPCR validated the success delivery (Figure 7A). Moreover, by Transwell assays we observed an increase in the number of invaded cells after *miR-206* was knocked-down (Figure 7B). Therefore, we constructed cells with simultaneous downregulation of *miR-206* and *AKAP13* (Figure 7C). The cells were cultured in Transwell chambers for 24 h, and the invasive cells were detected. Inhibition of *miR-206* and *AKAP13* reduced invasive cells versus suppression of *miR-206* alone (Figure 7D). Cells after co-transfection were injected into mice, and the results demonstrated the tumor formation rate in mice slowed down (Figure 7E), occurring concomitant with reduced tumor weight (Figure 7F). CD45 positivity in mouse tumor tissues revealed a significant reduction in AML cells after simultaneous downregulation of *miR-206* and *AKAP13* (Figure 7G). Poor AKPAP13 expression reversed the effect of *miR-206* inhibitor to decrease the number of metastatic liver nodules (Figure 7H) and to reduce activity of CD45-positive cells in metastatic tissues (Figure 7I). Thus, *miR-206* downregulation promoted cell invasion, but *AKAP13* silencing inhibited invasive ability caused by downregulation of *miR-206*.

ZNF667-as Exerts Pro-Tumorigenic Effects in AML by Sponging miR-206

ZNF667-AS1 has been indicated to competitively bind to miR-93-3p, which directly targeted PEG3 to involve in cervical cancer development.[8] Therefore, we postulated that *ZNF667-AS1* modulated the progression of AML in a similar manner. As predicted by lncATLAS (http://lncatlas.crg.eu/), *ZNF667-AS1* was mainly distributed in the cytoplasm in most cells (Figure 8A). We found *ZNF667-AS1* was principally localized in the cytoplasm of AML cells (Figure 8B) through subcellular fractionation location assay, and we further verified *ZNF667-AS1* localization results in the cytoplasm through the FISH experiment (Figure 8C). So, we predicted the possible binding miRNAs of *ZNF667-AS1* by RNA22. A total of four miRNAs were screened out and pCR quantification of candidate target miRNAs revealed that only *miR-206* showed high expression in THP-1 cells with poor expression of *ZNF667-AS1* (Figure 8D). We then verified the targeting relationship between *ZNF667-AS1* and *miR-206* in cells by dual-

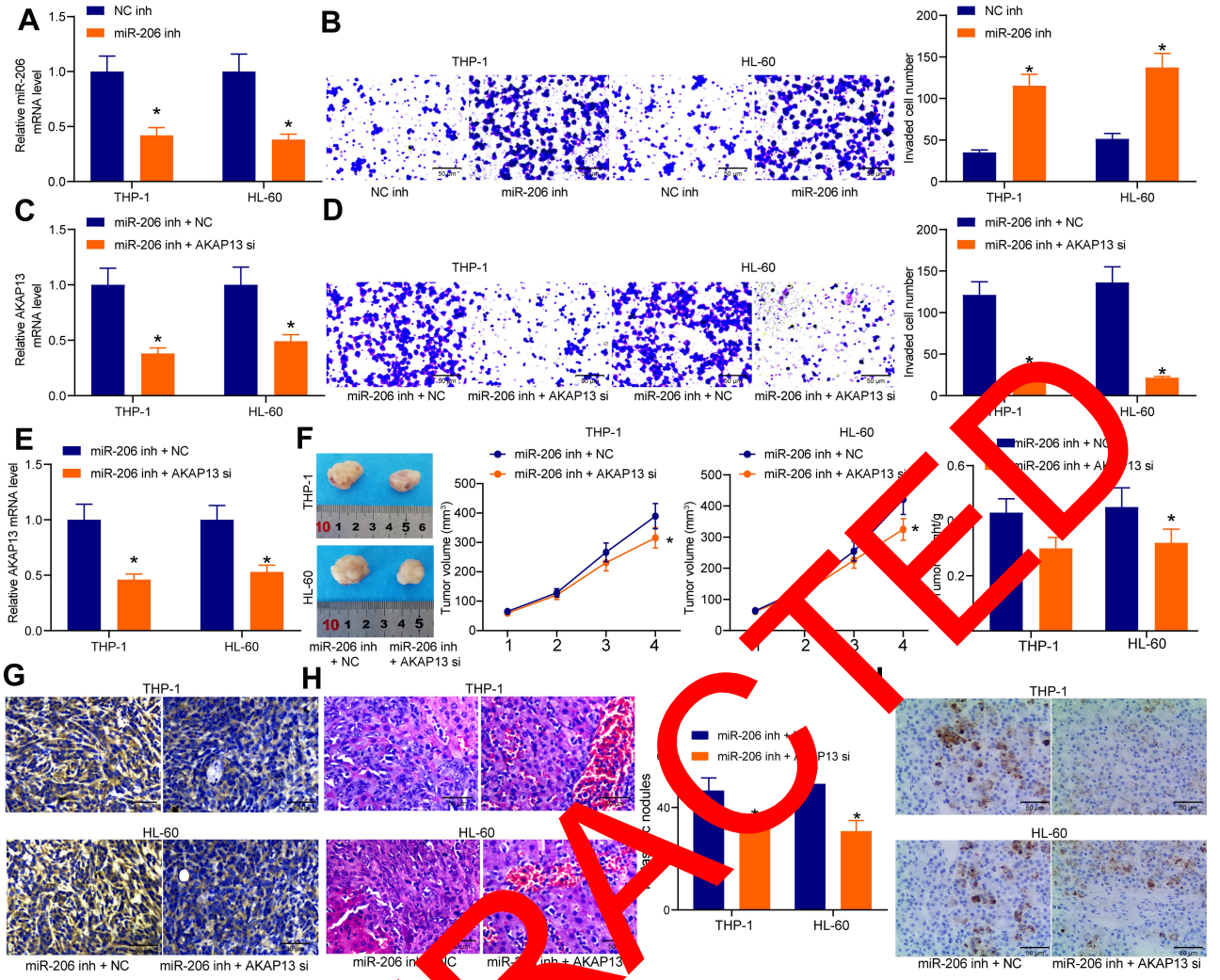

Figure 7 *AKAP13* silencing hampers the AML cell aggressiveness in the presence of miR-206 inhibitor. (**A**) RT-qPCR detection of *miR-206* expression in response to *miR-206* inh transfection (*$p < 0.05$ according to the two-way ANOVA); (**B**) Transwell assay of cell invasion (*$p < 0.05$ according to two-way ANOVA). AML cells were co-transfected with *miR-206* inh plus *AKAP13* si or NC. (**C**) RT-qPCR detection of *AKAP13* mRNA expression in AML cells after co-transfection (*$p < 0.05$ according to the two-way ANOVA); (**D**) Transwell assay of cell invasion after co-transfection (*$p < 0.05$ according to two-way ANOVA); (**E**) RT-qPCR detection of *AKAP13* mRNA expression in tumor tissues; (**F**) Tumor volume and tumor weight in mice (*$p < 0.05$ according to two-way ANOVA); (**G**) Immunohistochemical staining of CD45 protein in mouse tumor tissues; (**H**) HE staining of liver metastatic nodules in mice (*$p < 0.05$ according to two-way ANOVA); (**I**) Immunohistochemical staining of CD45 protein in liver metastatic nodules. Values are shown as the means ± SD of three separate experiments (n = 3).

luciferase reporter assays (Figure 8E). To find *miR-206* downstream genes, we predicted the target genes of miR-206 by RNA22. Kyoto Encyclopedia of Genes and Genomes (KEGG) analysis of the target genes of *miR-206* revealed that all genes were enriched in the Wnt/β-catenin pathway (Figure 8F). While *AKAP13* was identified by dual-luciferase assays as a target gene of *miR-206* and also enriched in the Wnt/β-catenin pathway (Figure 8G). Detection of *AKAP13* expression in cells with *miR-206* inhibitor revealed that downregulation of *miR-206* significantly increased *AKAP13* expression in the cells (Figure 8H). These findings illustrated that the binding of *ZNF667-AS1* to *miR-206* could modulate the *AKAP13* expression in AML cells.

ZNF667-AS1 Mediates the Wnt/β-Catenin Pathway

The Wnt/β-catenin pathway activities were finally detected in cells. Through Western blot detection of β-catenin and cyclin D1 expression, we observed that *ZNF667-AS1* downregulation impaired the Wnt/β-catenin pathway in cells, while *miR-206* inhibitor partially restored pathway activity. While silencing of *AKAP13* flattened the promotive role of *miR-206* inhibitor on the Wnt/β-catenin pathway induction (Figure 9). By examining Wnt/β-catenin

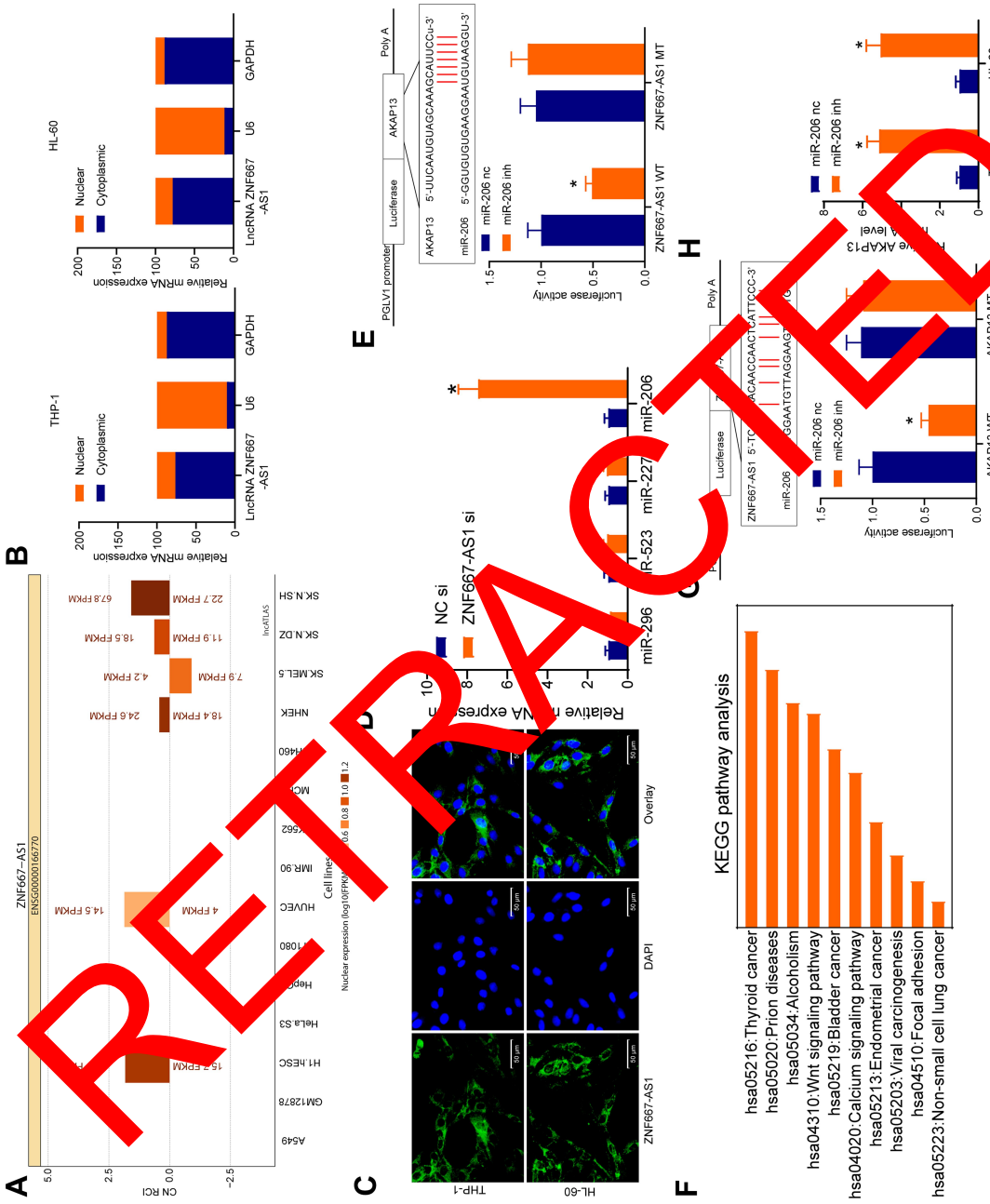

Figure 8 *ZNF667-AS1* inhibits *miR-206* expression and regulates invasion of AML cells. (**A**) lncATLAS prediction of *ZNF667-AS1* cell localization; (**B**) Detection of *ZNF667-AS1* expression in cytoplasm and nucleus by subcellular fractionation location assay (*$p < 0.05$ according to two-way ANOVA); (**C**) FISH localization of *ZNF667-AS1*; (**D**) RT-qPCR detection of binding miRNA expression in cells transfected with *ZNF667-AS1* si (*$p < 0.05$ according to two-way ANOVA); (**E**) Dual-luciferase reporter assay identification of the regulatory relationship between *ZNF667-AS1* and *miR-206* (*$p < 0.05$ according to two-way ANOVA); (**F**) KEGG pathway analysis of the pathway enrichment of *miR-206* target genes; (**G**) dual-luciferase reporter assay identification of the regulatory relationship between *miR-206* and *AKAP13* (*$p < 0.05$ according to two-way ANOVA); (**H**) the mRNA expression of AKAP13 in response to miR-206 inhibitor by RT-qPCR (*$p < 0.05$ according to two-way ANOVA). Values are shown as the means ± SD of three separate experiments.

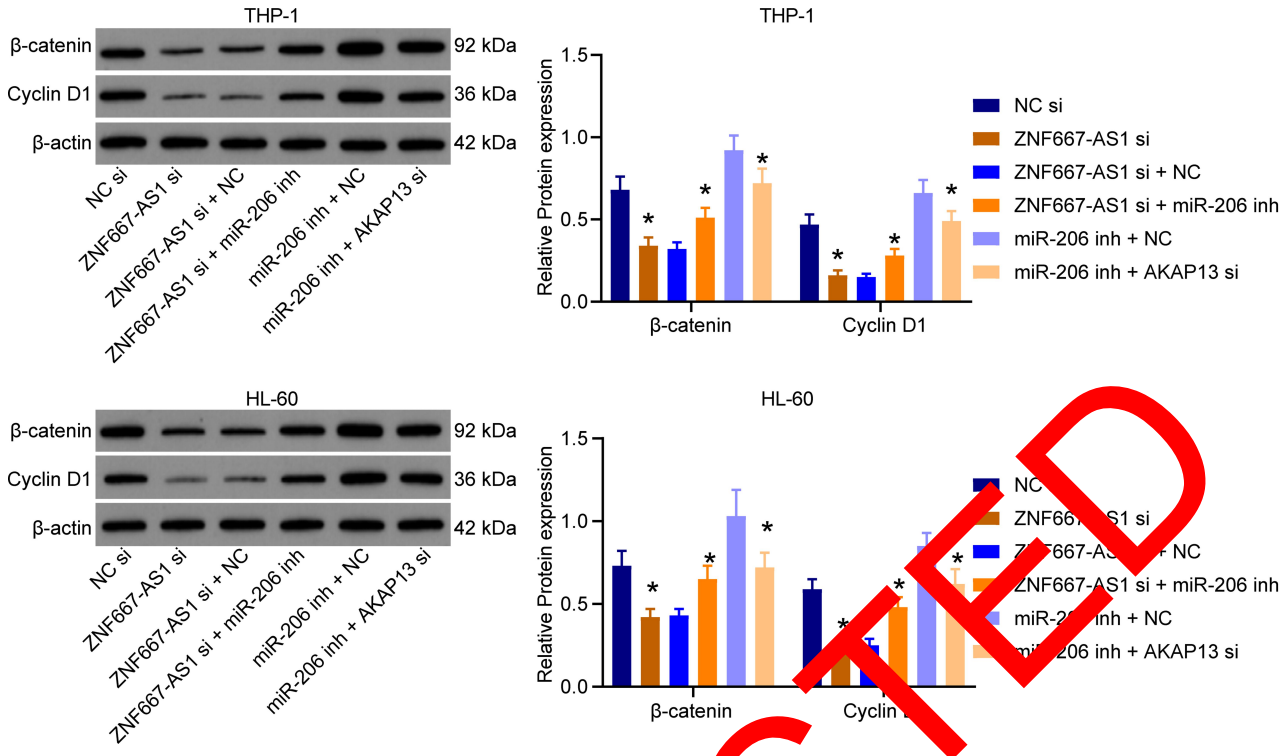

Figure 9 *ZNF667-AS1* promotes the Wnt/β-catenin signaling induction in AML cells via the *miR-206*/AKAP13 axis. The protein expression of β-catenin and cyclin D1 in AML cells after transfection (*$p < 0.05$ according to two-way ANOVA). Values are shown as the means ± SD of three separate experiments.

pathway-related proteins, we found that *ZNF667-AS1* regulates AML cell activity through *miR-206* regulation of *AKAP13* and activation of the Wnt/β-catenin pathway.

Discussion

AML is the most common acute leukemia in the population of adults, and the pathophysiology of this disease is just in ferment at the cellular and molecular levels, and effective biomarkers are of paramount importance for risk stratification and treatment of AML patients.[14] Interestingly, the investigation of lncRNAs suggested that ZNF571-AS1 may exert prognostic functions in AML, while the underlying mechanism of action has not been well characterized yet.[15] In this study, we validate the possible prognostic role of *ZNF667-AS1* in AML. Initially, we observed that *ZNF667-AS1* expression was distinctly overexpressed in bone marrow of AML patients. Furthermore, *ZNF667-AS1* expression displayed a high accuracy for diagnosing AML from healthy controls by a ROC curve. More importantly, the results of Kaplan-Meier analyses revealed that AML patients with high *ZNF667-AS1* expression demonstrated a shorter overall survival. As a consequence, our findings preliminarily indicated *ZNF667-AS1* as a prognostic factor for AML. However, further researches on greater number of patients are required to better verify of our findings.

In the current work, we herein excavated the possible effects of *ZNF667-AS1* on the proliferation and invasiveness of THP-1 and HL-60 cells and nude mice. The data from functional experiments including MTT, EdU, flow cytometry, Transwell and in vivo assays established that *ZNF667-AS1* knockdown suppressed the cell proliferation and invasiveness and tumor growth and liver metastases, suggesting that *ZNF667-AS1* functioned as a tumor-initiating lncRNA in AML. Investigation involving competing endogenous RNA (ceRNA), which are endogenous transcripts that share the same miRNA response elements and mediate each other by diminishing miRNA availability via competing for shared miRNAs, has been outlined in carcinogenesis.[16] When mRNA competes to miRNAs, its stability decreases, the translation process is impaired, and gene expression is altered, by which various lncRNAs participate in the modulation of mRNA coding function.[17] The ceRNA network plays an important role in a wide range of physiological and pathological processes, including AML.[18] To figure out whether *ZNF667-AS1* participated in AML through ceRNA mechanism, subcellular fractionation location assay and FISH assays were carried out, illustrating that *ZNF667-AS1* mainly

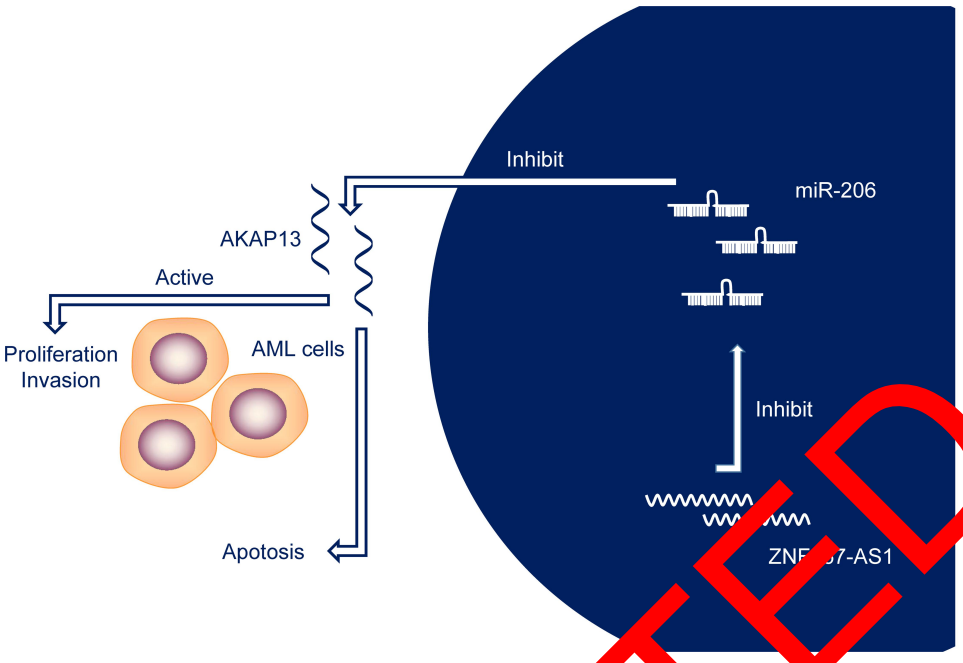

Figure 10 Schematic diagram of the relevance of *ZNF667-AS1* in AML. *ZNF667-AS1* positively regulated *AKAP13* expression by interacting with *miR-206*, thereby leading to cell proliferation and invasion.

distributed in the cytoplasm. The results of RNA22 prediction and dual-luciferase reporter assays showed that *ZNF667-AS1* bound to *miR-206*. Functional assays revealed that inhibition of *miR-206* rescued the function of ZNF667-AS1 silencing on the proliferation and invasion of AML cells. Overall, our findings displayed that *ZNF667-AS1* knockdown hampered AML cell proliferation and invasiveness through *miR-206*. Likewise, *miR-206* has been suggested to be mediated by different lncRNAs in various malignances, including neonatal neuroblastoma,[19] head and neck squamous cell carcinoma[20] in addition to hepatocellular carcinoma.[21] Also, *miR-206* has been validated to exhibit a high accuracy for diagnosing AML from healthy controls by ROC curve in our study.

Additionally, *miR-206* was found to target *AKAP13* to suppress AML cell proliferation and invasion. AKAP13 mRNA expression was observed by Toaldo et al to be linked to poor prognosis in patients with metastatic breast cancer receiving tamoxifen.[22] Likewise, *AKAP13*, notably overexpressed in AML patients, showed good diagnostic effects in AML in our study. Functional assays revealed that silencing of *AKAP13* could flatten the stimulative role of *miR-206* inhibitor in cell proliferation and invasion as well as tumor growth and liver metastasis. Lastly, *ZNF667-AS1* silencing was observed to block the Wnt/β-catenin signaling induction in AML cells, as evidenced by lowered expression of β-catenin and cyclin D1 at protein level. A previous review highlighted that the connections between lncRNAs, with specific expression patterns in different cancer tissues, and the Wnt/β-catenin signaling, showing potentials as new biomarkers and therapeutic targets.[23] While inhibition of *miR-206* partially restored the activity of the pathway. Cyclin D1 has been substantiated as a downstream target of *miR-206* in various cancers, including ovarian cancer,[24] melanoma,[25] in addition to clear-cell renal cell carcinoma.[26] Further Western blot assays also corroborated that *AKAP13* silencing impaired the Wnt/β-catenin signaling induction in the presence of *miR-206* inhibitor. In line with our study, *miR-206* was observed to attenuate glioma cell proliferation, migration and invasion through disrupting the Wnt/β-catenin signaling by targeting Frizzled 7 mRNA.[27]

Overall, this study found that *ZNF667-AS1* may be an onco-lncRNA in AML. The results of subsequent mechanistic studies displayed *ZNF667-AS1* enhanced the activation of the *AKAP13*/Wnt/β-catenin signaling by interacting with *miR-206* (Figure 10). The interaction between *ZNF667-AS1* and *miR-206* plays an important part in the proliferation and invasiveness of AML. In addition, we showed that *ZNF667-AS1*, *miR-206* and *AKAP13* may become attractive prognostic biomolecules for AML, which may offer new avenues for the research on molecular mechanisms of AML.

Disclosure

The authors declare no conflicts of interest.

References

1. Papaemmanuil E, Gerstung M, Bullinger L, et al. Genomic classification and prognosis in acute myeloid leukemia. *N Engl J Med*. 2016;374(23):2209–2221. doi:10.1056/NEJMoa1516192
2. Garzon R, Volinia S, Papaioannou D, et al. Expression and prognostic impact of lncRNAs in acute myeloid leukemia. *Proc Natl Acad Sci U S A*. 2014;111(52):18679–18684. doi:10.1073/pnas.1422050112
3. Robak T, Wierzbowska A. Current and emerging therapies for acute myeloid leukemia. *Clin Ther*. 2009;31(Pt 2):2349–2370. doi:10.1016/j.clinthera.2009.11.017
4. Wouters BJ, Delwel R. Epigenetics and approaches to targeted epigenetic therapy in acute myeloid leukemia. *Blood*. 2016;127(1):42–52. doi:10.1182/blood-2015-07-604512
5. Yang D, Zhang X, Zhang X, Xu Y. The progress and current status of immunotherapy in acute myeloid leukemia. *Ann Hematol*. 2017;96(12):1965–1982. doi:10.1007/s00277-017-3148-x
6. Xiao H, Liang S, Wang L. Competing endogenous RNA regulation in hematologic malignancies. *Clin Chim Acta*. 2020;509:108–116. doi:10.1016/j.cca.2020.05.045
7. Zhang R, Huo C-H. Long noncoding RNA SOCS2-AS promotes leukemogenesis in FLT3-ITD+ acute myeloid leukemia through miRNA-221. *Onco Targets Ther*. 2020;13:2925–2934. doi:10.2147/OTT.S222734
8. Li Y-J, Yang Z, Wang -Y-Y, Wang Y. Long noncoding RNA ZNF667-AS1 reduces tumor invasion and metastasis in cervical cancer by counteracting microRNA-93-3p-dependent PEG3 downregulation. *Mol Oncol*. 2019;13(11):2375–2392. doi:10.1002/1878-0261.12565
9. Zhuang L, Ding W, Ding W, Zhang Q, Xu X, Xi D. lncRNA ZNF667-AS1 (NR_036521.1) inhibits the progression of colorectal cancer via regulating ANK2/JAK2 expression. *J Cell Physiol*. 2020. doi:10.1002/jcp.30004
10. El-Khazragy N, Esmaiel MA, Mohamed MM, Hassan N. Upregulation of long noncoding RNA Lnc-IRF2-3 and Lnc ZNF667-AS1 is associated with poor survival in B-chronic lymphocytic leukemia. *Int J Lab Hematol*. 2020;42(3):284–29 doi: 1111/ijlh.13167
11. Liu H, Wu H, Qin X. MicroRNA-206 serves as a mor sup in pediatric acute myeloid leukemia by targeti Cyc D1 *athol Res Pract*. 2019;215(10):152554. doi:10.1016 prp.2019.1 54
12. Hu JK, Wang L, Li Y, et al. The mRN protein expr on of A-kinase anchor proteins 13 in human olorec cancer. *Clin Lab Med*. 2010;10(1):41–49. doi:10.1007/ 0238-009-00 x
13. Raponi M, Harousseau JL, L cet JE, et al. Ide ication of molecular predictors of respo e in a st dy of tipifarnib treatment in relapsed and refractory ute my genous leukemia. *Clin Cancer Res*. 2007;13(7):2254–220 do 0.1158/107 -0432.CCR-06-2609
14. Prada-Arismendy A rroyav C, Roth berger S. Molecular biomarkers in a e mye d leuke a. *od Rev*. 2017;31(1):63–76. doi:10.101 blre.201 8.005
15. Pan JQ, Zhang YQ, Wang JH, Xu P, Wang W. lncRNA co-expression network model for the prognostic analysis of acute myeloid leukemia. *Int J Mol Med*. 2017;39(3):663–671. doi:10.3892/ijmm.2017.2888
16. Qi X, Lin Y, Chen J, Shen B. Decoding competing endogenous RNA networks for cancer biomarker discovery. *Brief Bioinform*. 2020;21(2):441–457. doi:10.1093/bib/bbz006
17. Cheng Y, Su Y, Wang S, et al. Identification of circRNA-lncRNA-miRNA-mRNA competitive endogenous RNA network as novel prognostic markers for acute myeloid leukemia. *Genes (Basel)*. 2020;11:8. doi:10.3390/genes11080868
18. Wang JD, Zhou HS, Tu XX, et al. Prediction of competing endogenous RNA coexpression network as prognostic markers in AML. *Aging (Albany NY)*. 2019;11(10):3333–3347. doi:10.18632/aging.101985
19. Pan J, Zhang D, Zhang J, Qin P, Wang J A RMRP silence curbs neonatal neuroblastoma progressi by regula g microRNA-206/tachykinin-1 receptor axis via i tivating extrac ular signal-regulated kinases. *Cancer Biol er*. 2019;2):653–665. doi:10.1080/15384047.2018.1 0568
20. Li T, Qin Y, Zhen Z, e dl. Long non-c ng NA HOTAIR/microRNA-206 sponge gulates S C2 and fu er influences cell biological functions in hea nd ck squam s cell carcinoma. *Cell Prolif*. 2019;52(5 12651. d 0.1111/cp 2651
21. Tu J, Zhao Z M, et al. LINC 0707 ontributes to hepatocellular carcinoma ogres via sponging iR-206 to increase CDK14. *J Cell Physiol*. 2019;23):10615–10624. doi:10.1002/jcp.27737
22. Benti do C, Alexi Beelen K, et al. Protein kinase A-induced ta oxifen resistance is me iated by anchoring protein AKAP13. *MC Cancer*. 20 ;15:588. doi:10.1186/s12885-015-1591-4
23. XY, Hou PF, TT, et al. The roles of Wnt/beta-catenin signaling pa way related ncRNAs in cancer. *Int J Biol Sci*. 2018;14(14). 201 doi:10.7150/ijbs.27977
24. Chang L, Guo R, Yuan Z, Shi H, Zhang D. LncRNA HOTAIR s es CCND1 and CCND2 expression by sponging miR-206 in ovarian cancer. *Cell Physiol Biochem*. 2018;49(4):1289–1303. doi:10.1159/000493408
25. Georgantas RW 3rd, Streicher K, Luo X, et al. MicroRNA-206 induces G1 arrest in melanoma by inhibition of CDK4 and cyclin D. *Pigment Cell Melanoma Res*. 2014;27(2):275–286. doi:10.1111/pcmr.12200
26. Xiao H, Xiao W, Cao J, et al. miR-206 functions as a novel cell cycle regulator and tumor suppressor in clear-cell renal cell carcinoma. *Cancer Lett*. 2016;374(1):107–116. doi:10.1016/j.canlet.2016.01.032
27. Zhou F, Cao W, Xu R, et al. MicroRNA-206 attenuates glioma cell proliferation, migration, and invasion by blocking the WNT/beta-catenin pathway via direct targeting of Frizzled 7 mRNA. *Am J Transl Res*. 2019;11(7):4584–4601.